ORIGINAL ARTICLE

Enhanced nuclear localization of phosphorylated MLKL predicts adverse events in patients with dilated cardiomyopathy

Yugo Fujita[1][†], Toshiyuki Yano[1][†], Hiromitsu Kanamori[2], Daigo Nagahara[1], Atsuko Muranaka[1], Hidemichi Kouzu[1], Atsushi Mochizuki[1], Masayuki Koyama[1,3], Nobutaka Nagano[1], Takefumi Fujito[1], Ryo Nishikawa[1], Naoyuki Kamiyama[1], Marenao Tanaka[1], Atsushi Kuno[1,4], Masaya Tanno[1] and Tetsuji Miura[1,5]* [ID]

[1]*Department of Cardiovascular, Renal and Metabolic Medicine, Sapporo Medical University School of Medicine, Sapporo, 060-8543, Japan;* [2]*Department of Cardiology, Gifu University Graduate School of Medicine, Gifu, Japan;* [3]*Department of Public Health, Sapporo Medical University School of Medicine, Sapporo, Japan;* [4]*Department of Pharmacology, Sapporo Medical University School of Medicine, Sapporo, Japan; and* [5]*Department of Clinical Pharmacology, Faculty of Pharmaceutical Sciences, Hokkaido University of Science, Sapporo, Japan*

Abstract

Aims   The role of necroptosis in dilated cardiomyopathy (DCM) remains unclear. Here, we examined whether phosphorylation of mixed lineage kinase domain-like protein (MLKL), an indispensable event for execution of necroptosis, is associated with the progression of DCM.

Methods and results   Patients with DCM (n = 56, 56 ± 15 years of age; 68% male) were enrolled for immunohistochemical analyses of biopsies. Adverse events were defined as a composite of death or admission for heart failure or ventricular arrhythmia. Compared with the normal myocardium, increased signals of MLKL phosphorylation were detected in the nuclei, cytoplasm, and intercalated discs of cardiomyocytes in biopsy samples from DCM patients. The phosphorylated MLKL (p-MLKL) signal was increased in enlarged nuclei or nuclei with bizarre shapes in hypertrophied cardiomyocytes. Nuclear p-MLKL level was correlated negatively with septal peak myocardial velocity during early diastole (r = −0.327, P = 0.019) and was correlated positively with tricuspid regurgitation pressure gradient (r = 0.339, P = 0.023), while p-MLKL level in intercalated discs was negatively correlated with mean left ventricular wall thickness (r = −0.360, P = 0.014). During a median follow-up period of 3.5 years, 10 patients (18%) had adverse events. To examine the difference in event rates according to p-MLKL expression levels, patients were divided into two groups by using the median value of nuclear p-MLKL or intercalated disc p-MLKL. A group with high nuclear p-MLKL level (H-nucMLKL group) had a higher adverse event rate than did a group with low nuclear p-MLKL level (L-nucMLKL group) (32% vs. 4%, P = 0.012), and Kaplan–Meier survival curves showed that the adverse event-free survival rate was lower in the H-nucMLKL group than in the L-nucMLKL group (P = 0.019 by the log-rank test). Such differences were not detected between groups divided by a median value of intercalated disc p-MLKL. In δ-sarcoglycan-deficient (Sgcd$^{−/−}$) mice, a model of DCM, total p-MLKL and nuclear p-MLKL levels were higher than in wild-type mice.

Conclusion   The results suggest that increased localization of nuclear p-MLKL in cardiomyocytes is associated with left ventricular diastolic dysfunction and future adverse events in DCM.

Introduction

Dilated cardiomyopathy (DCM) is characterized by impaired contraction of the left ventricle or both ventricles together with ventricular dilatation, and refractory pump failure and lethal ventricular arrhythmia are responsible for poor prognosis of DCM.[1–4] As mechanisms of cardiomyocyte death contributing to the progression of DCM, apoptosis and autophagic cell death have received attention. In contrast, the role of necroptosis of cardiomyocytes in DCM has not yet been characterized. Necroptosis is a type of programmed cell death triggered by activation of death receptors, toll-like receptors, or viral DNAs, which results in the activation of receptor-interacting protein kinase 3 (RIP3), leading to phosphorylation of mixed lineage kinase domain-like protein (MLKL) at Thr357/Ser358. Phosphorylated MLKL (p-MLKL) is translocated from the cytosol to the plasma membrane, where polymerized p-MLKL disrupts the plasma membrane, resulting in cell death with morphology of necrosis.[5–7] A large number of dead cardiomyocytes in DCM have morphology of necrosis.[8–10] However, whether the necrotic death of cardiomyocytes is induced by ischemic necrosis due to insufficient microcirculation or by necroptosis has not been clarified.

Several lines of recent evidence indicate that necroptotic signalling may contribute to the progression of chronic heart failure. First, canonical necroptotic signalling activated by tumour necrosis factor-α (TNF-α) has been shown to exist in cardiomyocytes.[11,12] Second, adverse ventricular remodelling after myocardial infarction was attenuated in RIP3-deficient mice, suggesting a detrimental role of necroptotic signalling in ventricular remodelling.[13] Third, a study using a model of systemic lupus erythematosus showed that MLKL-mediated necroptosis was involved in the production of autoantibodies and in tissue injuries.[14,15] The presence of circulating cardiac autoantibodies in DCM patients has been reported, although their pathogenic roles are still debated.[16] Finally, recent studies have shown that levels of caspase-8 and transforming growth factor β-activated kinase 1, negative regulators of necroptotic signalling, were down-regulated and that p-MLKL level was up-regulated in end-stage heart failure.[17,18] Despite these lines of circumstantial evidence from cell and animal experiments, there have been few studies on necroptosis in human heart failure.

The aim of this study was to determine whether MLKL phosphorylation is associated with ventricular remodelling and predicts prognosis in patients with DCM. We particularly focused on subcellular localization of p-MLKL in cardiomyocytes because a crucial role of nuclear–cytoplasmic shuttling of MLKL in pro-necroptotic signalling has been unveiled recently in addition to a well-established role of p-MLKL polymerized at the plasma membrane in execution of necroptosis.[19,20] Endomyocardial biopsy (EMB) samples from DCM patients and also the myocardium of δ-sarcoglycan-deficient (Sgcd$^{-/-}$) mice were used in the present study to examine the associations of change in myocardial p-MLKL expression with ventricular function and outcomes in patients with DCM.
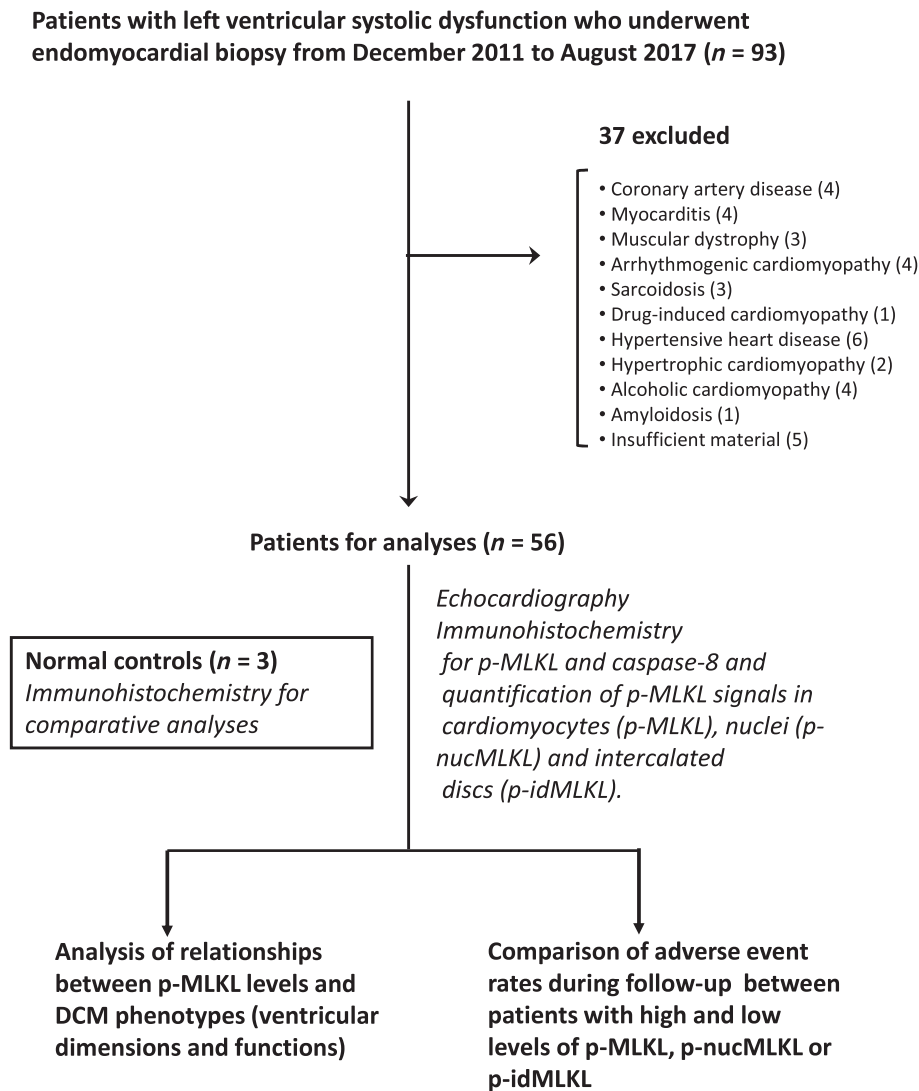
Methods

Study subjects

Consecutive DCM patients in whom EMB was performed during the period from 1 December 2011 to 31 August 2017 (*Figure 1*) were retrospectively enrolled. The decision to perform EMB was based on clinical indication as reported previously.[21] DCM was diagnosed according to Position Statement of the ESC Working Group.[22] Exclusion criteria were coronary artery disease, myocarditis including inflammatory DCM defined as more than 14/mm^2 of CD45-positive cells,[23] muscular dystrophy, arrhythmogenic cardiomyopathy, sarcoidosis, drug-induced cardiomyopathy, hypertensive heart disease, hypertrophic cardiomyopathy, alcoholic cardiomyopathy, and amyloidosis, which were diagnosed on the basis of clinical, radiographic, and histological findings. Patients whose myocardial biopsy samples were not suitable for immunohistochemical analyses were also excluded. Human kidney biopsy tissues were obtained from eight patients with kidney diseases including lupus nephritis for the purpose of diagnosis. Three cases of normal human myocardial tissues were obtained from US Biomax (Rockville, MD, #BC30013). This study was conducted in strict adherence with the principles of the Declaration of Helsinki and was approved by the institutional ethics committee of Sapporo Medical University Hospital (Numbers 302-25, 302-3741).

Echocardiography

Transthoracic echocardiography and tissue Doppler echocardiography (TDE) were performed using Vivid 7 or Vivid E9 (GE Healthcare, Tokyo, Japan) as previously reported.[24] Two-dimensional echocardiography was performed using standard echocardiographic views including parasternal long-axis and apical four-chamber, three-chamber, and two-chamber views from a left lateral decubitus position. The left ventricular (LV) ejection fraction (LVEF, %) was calculated using the biplane modified Simpson's method. Transmitral flow velocities were determined by pulsed-wave Doppler echocardiography, and mitral flow parameters, including peak velocities during early (E) and late diastole (A) and deceleration time of E, were measured. The pressure gradient of tricuspid regurgitation (TRPG) was calculated by applying the simplified Bernoulli equation: TRPG = $4v^2$ (v = peak velocity of tricuspid regurgitation, m/s).

Tissue Doppler echocardiography from the apical four-chamber view was recorded using a frame rate between 80 and 120 frames/s. A sample volume was placed at the

Figure 1 Flow chart of inclusion of patients and study protocol. To examine the difference in DCM phenotypes and adverse event rates according to p-MLKL expression levels, patients were classified into subgroups using median p-MLKL level as follows: a high p-MLKL level group (H-MLKL) and a low p-MLKL level group (L-MLKL); a high nuclear p-MLKL level group (H-nucMLKL) and a low nuclear p-MLKL level group (L-nucMLKL); and a high interca-lated disc p-MLKL level group (H-idMLKL) and a low intercalated disc p-MLKL level group (L-idMLKL). Normal myocardial samples from three subjects were used for comparison with samples from DCM patients.

Patients with left ventricular systolic dysfunction who underwent endomyocardial biopsy from December 2011 to August 2017 (*n* = 93)

37 excluded

- Coronary artery disease (4)
- Myocarditis (4)
- Muscular dystrophy (3)
- Arrhythmogenic cardiomyopathy (4)
- Sarcoidosis (3)
- Drug-induced cardiomyopathy (1)
- Hypertensive heart disease (6)
- Hypertrophic cardiomyopathy (2)
- Alcoholic cardiomyopathy (4)
- Amyloidosis (1)
- Insufficient material (5)

Patients for analyses (*n* = 56)

Echocardiography
Immunohistochemistry
for p-MLKL and caspase-8 and
quantification of p-MLKL signals in
cardiomyocytes (p-MLKL), nuclei (p-
nucMLKL) and intercalated
discs (p-idMLKL).

Normal controls (*n* = 3)
Immunohistochemistry for
comparative analyses

Analysis of relationships between p-MLKL levels and DCM phenotypes (ventricular dimensions and functions)

Comparison of adverse event rates during follow-up between patients with high and low levels of p-MLKL, p-nucMLKL or p-idMLKL

medial annulus in the apical four-chamber view, and peak myocardial velocity during early diastole (e′) was measured. Tricuspid annular plane systolic excursion was measured by two-dimensional echocardiography-guided M-mode record-ing from the apical four-chamber view.

Histological and immunohistochemical analyses of myocardial biopsy samples

In EMB, 2–4 samples were obtained from the right interven-tricular septum in each patient as previously described.[25] Biopsy samples were fixed in 10% buffered formalin, sec-tioned into 3-μm-thick slices, and stained with haematoxylin and eosin and Masson's trichrome. Images were obtained un-der a microscope (BZ-X700 series, Keyence Corporation, Osaka, Japan) and reconstructed using the image-joint pro-gram of BZ-X analyzer software (Keyence Corporation). The cardiomyocyte size and fibrosis areas were analysed in the entire myocardial field of each EMB sample (×400 magnifica-tion) using BZ-X analyzer software. The cardiomyocyte size was defined as the transverse diameter of cardiomyocytes at the level of the nucleus.[26] Using sections stained with Masson's trichrome, areas occupied by collagen (stained in blue) were quantified as fibrosis areas and expressed as per-centages of the total area (i.e. sum of fibrosis area and

cardiomyocyte area).[25] The number of infiltrating cells stained with anti-CD45 antibodies (working dilution, N1514, Dako) was counted and expressed as the number of CD45-positive cells/mm^2.

Immunostaining after antigen retrieval was performed using a peroxidase-based technique with a Dako EnVision$^+$ kit including Dako EnVision$^+$ System-HRP Labelled Polymer Anti-Rabbit (K4002) as a secondary antibody with diamino-benzidine as the chromogen. To analyse necroptotic signalling in cardiomyocytes, we used polyclonal antibodies against caspase-8 (1:4, PA121140, Invitrogen) and those against p-MLKL-Ser358 (1:50, ab208909, Abcam) as primary antibodies. ab208909 is an azide-free version of ab187091, a well-characterized antibody for detection of human p-MLKL-Ser358. The azide-free version appears suitable for HRP-based immunohistochemistry because sodium azide suppresses HRP enzyme activity. Rabbit immunoglobulin (1:1, N1699, Dako) as a negative control for a primary antibody and a blocking peptide for ab208909 (10 μg per 1 μg of ab208909, ab206929, Abcam) were used for validation of specific p-MLKL immunostaining. In pilot experiments, we also tried to immunostain total MLKL in EMB samples by four different anti-MLKL antibodies (LS-B13161, LifeSpan Bio-Sciences; ab184718, abcam; MA5-24846, Invitrogen; 66675-1-Ig, Proteintech), but unfortunately, the antibodies did not work in our samples. To minimize variations in dyeability, immunostaining was performed using an automated immuno-histochemical staining system (BOND-MAX, Leica Biosystems) by an investigator. The nuclei were counterstained with haematoxylin.

Quantification of mixed lineage kinase domain-like protein and caspase expressions in endomyocardial biopsy samples

Expression levels of signal proteins in EMB samples were determined by analysis in the entire myocardial field of each EMB sample (×400 magnification). The thresholds to detect areas stained with anti-caspase-8 antibodies and anti-p-MLKL antibodies were manually set according to a histogram of the signal intensity using BZ-X analyzer software in the analysis of each specimen. The areas stained with antibodies were automatically quantified using BZ-X analyzer software, and the percentage of the positive area in the total myocardial area was calculated. The number of p-MLKL-positive cardiomyocyte nuclei and total cardiomyocyte nuclei in myocardial sections were counted, and the percentage of p-MLKL-positive cardiomyocyte nuclei was calculated as shown in the left panels of *Figure 2*. Unexpectedly, we found that p-MLKL

Figure 2 Quantification of nuclear and intercalated disc p-MLKL levels. (A) The number of phosphorylated MLKL (p-MLKL)-positive cardiomyocyte nuclei and the number of total cardiomyocyte nuclei in myocardial sections were counted, and nuclear p-MLKL level was expressed as the percentage of the number of p-MLKL-positive cardiomyocyte nuclei to the number of total cardiomyocyte nuclei. Using the median value, that is, 25%, patients were classified into a high nuclear p-MLKL level group (H-nucMLKL) and a low nuclear p-MLKL level group (L-nucMLKL). (B) p-MLKL expression levels in the intercalated discs of cardiomyocytes were analysed in a field (200 × 200 μm) in which cardiomyocytes were sectioned longitudinally. Intercalated disc areas stained with anti-p-MLKL antibodies were selected and quantified using BZ-X analyzer software, and the percentage of the positive area to the total area of cardiomyocytes was calculated. Using the median value, that is, 0.38%, patients were classified into a high intercalated disc p-MLKL level group (H-idMLKL) and a low intercalated disc p-MLKL level group (L-idMLKL).
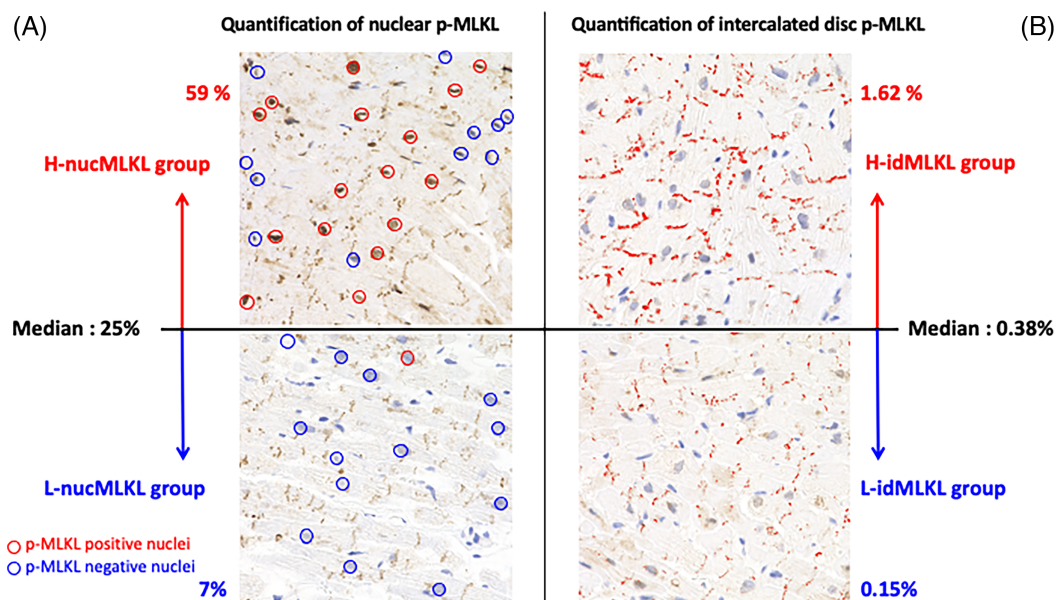
signals increased in the intercalated discs of cardiomyocytes (see the Results section). Thus, p-MLKL signals in 200 × 200 μm fields, in which cardiomyocytes were sectioned longitudinally, were quantified by using BZ-X analyzer software to calculate the percentage of the positive area to the total area of cardiomyocytes as shown in the right panels of *Figure 2*. p-MLKL signals in the intercalated discs were determined by subtracting p-MLKL signals in the nuclei from the total p-MLKL signals in the examined fields.

To examine the difference in DCM phenotypes according to p-MLKL expression levels, patients were divided into two groups by using the median value of total p-MLKL, nuclear p-MLKL (p-nucMLKL), or intercalated disc p-MLKL (p-idMLKL): a high p-MLKL level group (H-MLKL group) vs. a low p-MLKL level group (L-MLKL group), a high p-nucMLKL level group (H-nucMLKL group) vs. a low p-nucMLKL level group (L-nucMLKL group), and a high p-idMLKL level group (H-idMLKL group) vs. a low p-idMLKL level group (L-idMLKL group).

Clinical endpoint

The clinical endpoint was adverse events defined as a composite of all-cause death and hospitalization for heart failure and/or arrhythmia during the follow-up period from the day of discharge until 7 November 2019. Data for adverse events in the enrolled patients were obtained from medical records.

Validation of p-MLKL-Ser358 antibody by cell culture and immunoblotting

HT-29 cells, human colorectal adenocarcinoma cells, and C2C12 cells, an immortalized mouse myoblast cell line, were cultured in Dulbecco's modified Eagle's medium (4.5 g/L glucose) supplemented with 10% foetal bovine serum and antibiotics.[27,28] The protocol for induction of necroptosis in HT-29 cells and C2C12 cells was selected according to previous studies.[20,28,29] HT-29 cells were assigned to 3 or 6 h treatment with the combination of 50 ng/mL TNF-α (Sigma-Aldrich, St. Louis, MO), 1 μM BV6 (ApexBio, Houston, TX), and 20 μM Z-Val-Ala-DL-Asp-fluoromethylketone (zVAD, Promega, Madison, WI) or a vehicle. C2C12 cells were assigned to 4 or 8 h treatment with the combination of TNF-α and zVAD or a vehicle. To obtain whole-cell lysates, samples were homogenized in a lysis buffer (CelLytic M, Sigma-Aldrich), a protease inhibitor cocktail (Complete mini, Roche Molecular Biochemicals, Mannheim, Germany), and a phosphatase inhibitor cocktail (PhosSTOP, Roche Molecular Biochemicals). The homogenate was centrifuged at 13 000 *g* for 15 min to obtain the supernatant. Fractionation of the nuclei and cytosol was performed as previously described.[11] Protein concentration was determined using the Bradford assay. Equal amounts of proteins were electrophoresed on 15%

polyacrylamide gels and then blotted onto PVDF membranes (Millipore, Bedford, MA). After blocking had been performed with a TBS-T buffer containing 5% non-fat dry milk or 5% BSA, the blots were incubated with antibodies that recognize the following: human p-MLKL-Ser358 (ab208909, Abcam), mouse p-MLKL-Ser345 (MA5-32752, Thermo Fisher Scientific; ab196436, Abcam), human MLKL (ab184728, Abcam), mouse MLKL (ab243142, Abcam), p-RIP3-Thr231/Ser232 (ab222320, Abcam), RIP3 (#15828, Cell Signaling Technology), vinculin (V9131, Sigma-Aldrich), histone-H3 (ab1791, Abcam), and α-tubulin (T9026, Sigma-Aldrich). Immunoblotted proteins were visualized by using an Immobilon Western detection kit (Millipore, Billerica, MA).

Animal model of cardiomyopathy

In the present study, δ-sarcoglycan-deficient (Sgcd$^{-/-}$) mice were used as an animal model of DCM based on their similarities to human DCM.[30–35] Mutations in the human δ-sarcoglycan genes have been demonstrated in familial and sporadic cases of DCM,[30,31] and mutations in the δ-sarcoglycan gene have been shown to induce dilatation of both ventricles and contractile dysfunction, typical features of DCM, in mice and hamsters.[32–35] Sgcd$^{-/-}$ mice (B6.129-Sgcdtm1Mcn/J) were purchased from Jackson Laboratory (Bar Harbor, ME) and bred as previously reported.[29] Age-matched non-transgenic mice (C57BL/6J, CLEA Japan) served as wild-type (WT) controls. At 36 weeks of age, Sgcd$^{-/-}$ male mice and WT male mice were sacrificed, and their hearts were removed. The excised hearts were fixed in 10% buffered formalin, embedded in paraffin, and sectioned into 4-μm-thick slices. Immunostaining was performed using antibodies that recognize phosphorylation of MLKL at Ser345 (1:50, MA5-32752, Thermo Fisher Scientific; 1:50, ab196436, Abcam), corresponding to Ser358 in human MLKL, phosphorylation of RIP3 at Thr231 and Ser232 (1:50, ab222320, Abcam), and caspase-8 (1:4, PA121140, Invitrogen), and signals were quantified by the methods used for EMB samples. Echocardiography of mice was performed as previously reported.[29] This series of the study was approved by the institutional animal research committee of Gifu University.

Statistical analysis

Data are presented as means ± standard deviation, medians [inter-quartile range (IQR)], or percentages for variables. Differences in continuous variables between two groups were tested by Student's *t*-test or the Mann–Whitney *U* test. Differences in categorical variables between two groups were analysed by Fisher's test. Simple regression analysis was used for determining the relationships between signal levels of p-MLKL and clinical parameters. The normality of the

distribution of each variable was examined by using the Shapiro–Wilk test, and variables that were not normally distributed were log transformed for analyses. Survival curves were calculated by the Kaplan–Meier method and compared using the log-rank test. A probability value of <0.05 was considered to be statistically significant. Statistical analysis was performed using EZR software (Jichi Medical University, Saitama, Japan).

Results

Baseline characteristics

Of 93 patients initially screened, 37 patients were excluded by the exclusion criteria, and data for 56 patients were used for analyses as shown in *Figure 1*. As shown in *Table 1*, the mean age of the patients was 56 ± 15 years, and 68% of them were male. At the time of EMB, 18% of the patients had New York Heart Association (NYHA) Functional Class III or IV symptoms. Fourteen per cent of the patients had a family history of DCM, and 20% of the patients had episodes of fatal arrhythmia. Mean LVEF in the patients was 33 ± 11%, and median LV end-diastolic volume index (LVEDVI) was 91 mL/m^2 (IQR, 67–110 mL/m^2).

Validation of anti-p-MLKL-Ser358 antibody

Immunohistochemical staining with ab208909 for the detection of p-MLKL-Ser358 antibody was validated according to the statement published by the Histochemical Society.[36] First, the specificity of an antibody–antigen binding, that is, detection of the target molecule of the appropriate molecular size, was analysed using lysates of HT-29 cells, human colorectal adenocarcinoma cells, for immunoblotting because canonical necroptotic signalling has been shown to operate in HT-29 cells.[20,29] No signal was found in immunoblotting for p-MLKL-Ser358, a 53 kDa protein, in unstimulated HT-29 cell samples, and only one band signal for the 53 kDa protein was detected in TNF/BV6/zVAD-treated HT-29 cells, while total MLKL levels were comparable between the unstimulated cells and the TNF/BV6/zVAD-treated cells (Supporting Information, *Figure S1A* and *S1B*). The signal for the 53 kDa protein was also detected in nuclear and cytosol fractions extracted from TNF/BV6/zVAD-treated HT-29 cells (Supporting Information, *Figure S1C*). Second, positive controls of human biopsy samples were examined by the use of ab208909. Consistent with the results of an earlier study,[14] p-MLKL signals were detected in kidney biopsy tissues of lupus nephritis (Supporting Information, *Figure S2A* and *S2B*). The signal of p-MLKL in lupus nephritis was absent when rabbit immunoglobulins were used as a negative control for ab208909 (Supporting Information, *Figure S2C* and *S2D*), and the addi-

tion of a blocking peptide prior to the incubation with ab208909 abolished the signal of p-MLKL (Supporting Information, *Figure S3A* and *S3B*). Taken together, the results of the immunoblotting and immunostaining of biopsy samples of lupus nephritis indicate that ab208909 specifically detects phosphorylation of MLKL at Ser358 in human tissue samples.

p-MLKL and caspase-8 expression in myocardial tissues

Various degrees of cardiomyocyte hypertrophy together with nuclear enlargement and interstitial fibrosis were observed in the biopsy samples from all DCM patients (*Figure 3A* and *3B*). p-MLKL signals were detected in the nuclei, cytoplasm, and intercalated discs of cardiomyocytes, whereas they were barely detected in mononuclear cells localized in the myocardial interstitium (*Figure 3C* and *3D*). p-MLKL signals were particularly found in enlarged nuclei and nuclei with bizarre shapes in hypertrophied cardiomyocytes (*Figure 3E*). Increased p-MLKL signals were frequently observed in cardiomyocytes around patchy areas of fibrous scar, possibly suggesting a topographic relationship between p-MLKL-mediated cell death and replacement fibrosis. In contrast, p-MLKL signals were almost undetected in normal human samples (*Figure 3F* and Supporting Information, *Figure S4A–S4F*). Specificity of p-MLKL signals in immunostained samples was confirmed by the findings that the signals were not detected by rabbit immoglobulins and were completely lost by the addition of a blocking peptide prior to the incubation with ab208909 (*Figure 3G* and Supporting Information, *Figure S3C* and *S3D*). The distribution of caspase-8 signals was partly different from that of p-MLKL signals; caspase-8 signals were detected in the cytosol and intercalated discs, but not in the nuclei, of cardiomyocytes (*Figure 3H*).

Relationships of p-MLKL expression levels with clinical and histological parameters

There were no significant differences in age, sex, body mass index, NYHA functional class, blood pressure, and brain-type natriuretic peptide (BNP) level between groups according to p-MLKL expression levels (*Table 2*). The proportion of patients with a family history of cardiomyopathy and the proportion of patients receiving renin–angiotensin system inhibitors, beta-blockers, or aldosterone receptor antagonists at the time of EMB were also similar in the groups with different p-MLKL levels.

Results of simple linear regression analyses are presented in *Table 3*. p-MLKL level was not correlated with LVEF, LVEDVI, or LV mass index, while it was positively correlated with age ($r = 0.266$). p-nucMLKL level was correlated negatively with septal e' ($r = -0.327$) and was correlated positively

Table 1 Clinical characteristics

Baseline characteristics	
Age (years)	56 ± 15
Male, *n* (%)	38 (68%)
Body mass index (kg/m^2)	22.6 (19.6–25.1)
Heart rate (b.p.m.)	75.2 ± 18.5
Systolic blood pressure (mmHg)	116 ± 20
Family history of DCM, *n* (%)	8 (14%)
Hypertension, *n* (%)	17 (30%)
Diabetes mellitus, *n* (%)	16 (29%)
Dyslipidaemia, *n* (%)	21 (38%)
Chronic kidney disease, *n* (%)	19 (34%)
NYHA III or IV, *n* (%)	10 (18%)
Arrhythmia	
Fatal arrhythmia, *n* (%)	11 (20%)
NSVT, *n* (%)	28 (50%)
Atrial fibrillation, *n* (%)	21 (38%)
Device	
ICD, *n* (%)	13 (23%)
CRTD, *n* (%)	6 (11%)
Medication	
RASI, *n* (%)	23 (41%)
Beta-blocker, *n* (%)	38 (68%)
Loop diuretic, *n* (%)	33 (59%)
MRA, *n* (%)	26 (46%)
Amiodarone, *n* (%)	17 (30%)
Laboratory data	
BNP (pg/mL)	194 (80–505)
Albumin (g/dL)	3.9 ± 0.5
Total bilirubin (mg/dL)	0.8 (0.5–1.0)
eGFR (mL/min/1.73 m^2)	66.4 ± 21.9
Haemoglobin (g/dL)	13.8 ± 2.2
Echocardiography	
LVEF (%)	33 ± 11
LVEDVI (mL/m^2)	91 (67–110)
LVESVI (mL/m^2)	60 (38–81)
LVMI (g/m^2)	116 (101–140)
Mean LV wall thickness (mm^2)	9.4 (8.2–10.7)
Septal e' (cm/s)	4.5 (3.8–6.0)
E/septal e'	13.9 (11.0–18.8)
E/A	1.2 (0.7–2.2)
LAVI (mL/m^2)	47.3 ± 17.3
RAVI (mL/m^2)	25.8 (16.0–32.7)
TAPSE (mm)	17.5 ± 4.5
Pressure gradient of TR (mmHg)	24 (18–31)
Histological findings	
Fibrosis area (%)	7.2 (4.1–14.1)
Cardiomyocyte size (μm)	17.4 ± 3.5
CD45-positive cells (/mm^2)	3.4 (1.6–5.3)

A, mitral peak late diastolic filling velocity; BNP, brain natriuretic peptide; CD, cluster of differentiation; CRTD, cardiac resynchronization therapy defibrillator; DCM, dilated cardiomyopathy; E, mitral peak early diastolic filling velocity; e', mitral annular peak velocity during early diastole; eGFR, estimated glomerular filtration rate; ICD, implantable cardioverter defibrillator; LAVI, left atrial volume index; LV, left ventricular; LVEDVI, left ventricular end-diastolic volume index; LVEF, left ventricular ejection fraction; LVESVI, left ventricular end-systolic volume index; LVMI, left ventricular mass index; MRA, mineralocorticoid receptor antagonist; NSVT, non-sustained ventricular tachycardia; NYHA, New York Heart Association functional classification; RASI, renin–angiotensin system inhibitor; RAVI, right atrial volume index; TAPSE, tricuspid annular plane systolic excursion; TR, tricuspid regurgitation.
Data are presented as means ± standard deviation, median (inter-quartile range), or percentage for variables.

Figure 3 Representative images of histological and immunohistochemical staining. (A) Masson's trichrome staining. (B) Haematoxylin and eosin staining. Immunostaining for p-MLKL in patients with dilated cardiomyopathy (C–E) and a normal control (F). (G) A representative image of a tissue incubated with rabbit immunoglobulins as a substitute for a primary antibody. (H) Immunostaining for caspase-8.
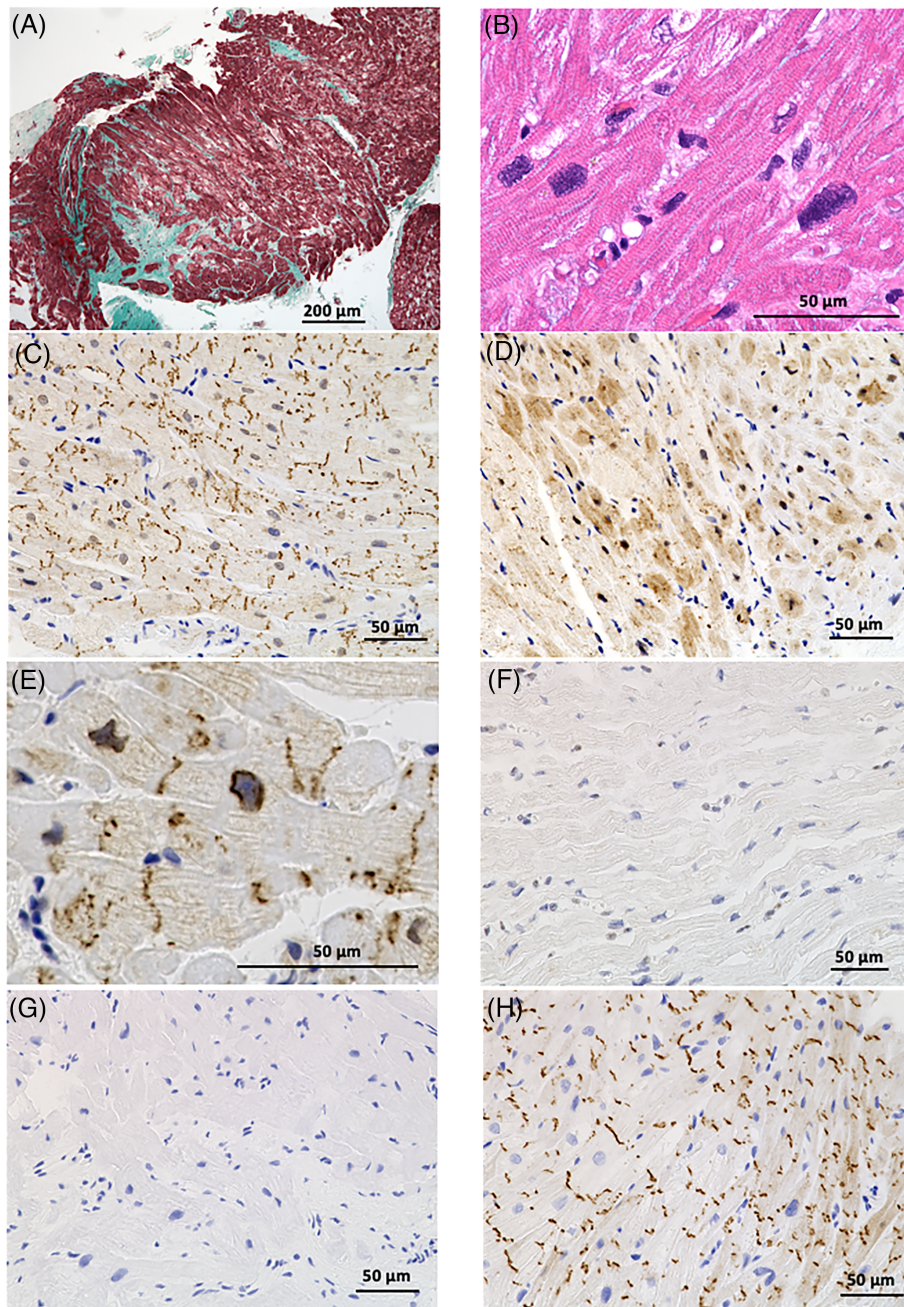
with TRPG (r = 0.339). p-idMLKL level was negatively correlated with mean LV wall thickness (r = −0.360). There was no significant relationship of the level of p-MLKL, p-idMLKL, or p-nucMLKL with cardiomyocyte size, fibrosis area, or number of CD45-positive cells. In contrast to our assumption, caspase-8 level was not correlated with any of the three indexes of p-MLKL expression.

Adverse event rates in DCM patients with different levels of p-MLKL

During a median 3.5 year period (IQR, 2.6–4.7 years), 10 patients (18%) had adverse events (all-cause death in four patients, readmission for heart failure in five patients, and readmission for ventricular arrhythmia in one patient). There was

Table 2 Clinical characteristics in p-MLKL subgroups

	All	p-MLKL			p-nucMLKL			p-idMLKL		
		L-MLKL	H-MLKL	P	L-nucMLKL	H-nucMLKL	P	L-idMLKL	H-idMLKL	P
Baseline characteristics										
Age (years)	56 ± 15	54 ± 15	58 ± 14	0.351	54 ± 15	59 ± 14	0.194	58 ± 14	56 ± 14	0.622
Male, n (%)	38 (68%)	19 (68%)	19 (68%)	1.000	22 (79%)	16 (57%)	0.152	19 (79%)	12 (50%)	0.069
Family history of DCM, n (%)	8 (14%)	3 (11%)	5 (18%)	0.705	5 (18%)	3 (11%)	0.705	3 (13%)	3 (13%)	1.000
Hypertension, n (%)	17 (30%)	6 (21%)	11 (39%)	0.245	7 (25%)	10 (36%)	0.562	7 (29%)	7 (29%)	1.000
Diabetes mellitus, n (%)	16 (29%)	8 (29%)	8 (29%)	1.000	9 (32%)	7 (25%)	0.768	5 (21%)	8 (33%)	0.517
Dyslipidaemia, n (%)	21 (38%)	10 (36%)	11 (39%)	1.000	10 (36%)	11 (39%)	1.000	9 (38%)	7 (29%)	0.760
Chronic kidney disease, n (%)	19 (34%)	11 (39%)	8 (29%)	0.573	9 (32%)	10 (36%)	1.000	10 (42%)	6 (25%)	0.359
NYHA III or IV, n (%)	10 (18%)	3 (11%)	7 (25%)	0.295	3 (11%)	7 (25%)	0.295	2 (8%)	7 (29%)	0.137
BNP (pg/mL)	194 (80–505)	183 (70–439)	209 (89–505)	1.000	212 (55–351)	172 (98–787)	0.346	230 (105–477)	178 (80–525)	0.865
Arrhythmia										
Fatal arrhythmia, n (%)	11 (20%)	6 (21%)	5 (18%)	1.000	5 (18%)	6 (21%)	1.000	6 (25%)	2 (8%)	0.245
NSVT, n (%)	28 (50%)	13 (46%)	15 (54%)	0.790	11 (39%)	17 (61%)	0.181	12 (50%)	13 (54%)	1.000
Atrial fibrillation, n (%)	21 (38%)	11 (39%)	10 (36%)	1.000	8 (29%)	13 (46%)	0.269	10 (42%)	10 (42%)	1.000
Medication										
RASI, n (%)	23 (41%)	10 (36%)	13 (46%)	0.587	10 (36%)	13 (46%)	0.587	13 (54%)	10 (42%)	0.564
Beta-blocker, n (%)	38 (68%)	19 (68%)	19 (68%)	1.000	19 (68%)	19 (68%)	1.000	18 (75%)	14 (58%)	0.359
Loop diuretic, n (%)	33 (59%)	16 (57%)	17 (61%)	1.000	15 (54%)	18 (64%)	0.587	13 (54%)	15 (63%)	0.770
MRA, n (%)	26 (46%)	13 (46%)	13 (46%)	1.000	12 (43%)	14 (50%)	0.789	11 (46%)	13 (54%)	0.773
Amiodarone, n (%)	17 (30%)	10 (36%)	7 (25%)	0.562	6 (21%)	11 (39%)	0.245	9 (38%)	6 (25%)	0.534
Adverse events										
Total adverse events, n (%)	10 (18%)	6 (21%)	4 (14%)	0.729	1 (4%)	9 (32%)	0.012	4 (17%)	5 (21%)	0.725
Death, n (%)	4 (7%)	2 (7%)	2 (7%)	1.000	1 (4%)	3 (18%)	0.611	1 (4%)	2 (8%)	0.609
Admission for heart failure, n (%)	5 (9%)	3 (11%)	2 (7%)	1.000	0 (0%)	5 (18%)	0.051	3 (13%)	2 (8%)	1.000
Admission for arrhythmia, n (%)	1 (2%)	1 (4%)	0 (0%)	1.000	0 (0%)	1 (4%)	1.000	0 (0%)	1 (4%)	0.490

BNP, brain natriuretic peptide; DCM, dilated cardiomyopathy; MRA, mineralocorticoid receptor antagonist; NSVT, non-sustained ventricular tachycardia; NYHA, New York Heart Association functional classification; p-idMLKL, intercalated disc p-MLKL; phospho-MLKL; p-nucMLKL, nuclear p-MLKL; RASI, renin–angiotensin system inhibitor.
Data are presented as means ± standard deviation, median (inter-quartile range), or percentage for variables.

Table 3 Simple regression analyses for p-MLKL

	p-MLKL level		p-nucMLKL level		p-idMLKL level	
	r	P	r	P	r	P
Age (years)	0.266	0.048	0.126	0.354	−0.042	0.775
Body mass index (kg/m^2)	−0.052	0.702	−0.065	0.635	−0.161	0.270
Heart rate (b.p.m.)	0.061	0.654	0.121	0.373	0.173	0.234
Systolic blood pressure (mmHg)	0.109	0.422	−0.087	0.523	−0.083	0.573
BNP (pg/mL)	0.058	0.685	0.150	0.292	0.035	0.821
LVEF (%)	0.056	0.681	−0.085	0.531	0.046	0.754
LVEDVI (mL/m^2)	−0.019	0.893	0.020	0.888	−0.102	0.506
LVESVI (mL/m^2)	−0.103	0.468	0.164	0.244	−0.088	0.567
LVMI (g/m^2)	−0.034	0.842	0.042	0.805	−0.263	0.146
Mean LV wall thickness (mm^2)	0.016	0.913	−0.126	0.367	−0.360	0.014
Septal e′ (cm/s)	0.064	0.654	−0.327	0.019	0.073	0.637
E/septal e′	0.092	0.529	0.208	0.151	0.117	0.462
E/A	−0.104	0.506	0.010	0.947	0.160	0.351
LAVI (mL/m^2)	−0.004	0.980	0.133	0.378	−0.099	0.549
RAVI (mL/m^2)	−0.013	0.936	−0.044	0.788	0.018	0.920
TAPSE (mm)	0.008	0.959	−0.036	0.816	0.167	0.311
Pressure gradient of TR (mmHg)	0.080	0.601	0.339	0.023	0.039	0.813
Fibrosis area (%)	0.017	0.902	−0.173	0.201	0.021	0.886
Cardiomyocyte size (μm)	−0.082	0.619	0.215	0.188	0.055	0.749
CD45-positive cells (/mm^2)	0.071	0.606	0.151	0.270	0.005	0.974
Caspase-8 positive area (%)	0.101	0.459	−0.094	0.493	−0.163	0.264

A, mitral peak late diastolic filling velocity; BNP, brain natriuretic peptide; CD, cluster of differentiation; E, mitral peak early diastolic filling velocity; e′, mitral annular peak velocity during early diastole; LAVI, left atrial volume index; LV, left ventricular; LVEDVI, left ventricular end-diastolic volume index; LVEF, left ventricular ejection fraction; LVESVI, left ventricular end-systolic volume index; LVMI, left ventricular mass index; MLKL, mixed lineage kinase domain like pseudokinase; p-idMLKL, intercalated disc p-MLKL; p-MLKL, phospho-MLKL; p-nucMLKL, nuclear p-MLKL; RAVI, right atrial volume index; TAPSE, tricuspid annular plane systolic excursion; TR, tricuspid regurgitation.

no significant difference in the rates of adverse events between the H-MLKL group and L-MLKL group or between the H-idMLKL group and L-idMLKL group. However, patients in the H-nucMLKL group had a significantly higher adverse event rate than did patients in the L-nucMLKL group (32% vs. 4%, *P* = 0.012, *Table 2*). Kaplan–Meier survival curves showed that the adverse event-free survival rate was significantly lower in the H-nucMLKL group than in the L-nucMLKL group (68% vs. 96%, *P* = 0.019, *Figure 4B*), whereas such a difference in the event-free survival rate was not found between the H-idMLKL and L-idMLKL groups (79% vs. 83%, *P* = 0.999, *Figure 4C*). In receiver operating characteristic curve analyses, the area under the curve (AUC) value for p-nucMLKL to predict adverse events was 0.826 [95% confidence interval (CI), 0.657–0.995]. This AUC value for p-nucMLKL was comparable with the AUC value for BNP (0.823; 95% CI, 0.688–0.958) and was larger than the AUC value for p-idMLKL (0.547; 95% CI, 0.300–0.795) as shown in *Figure 4D*.
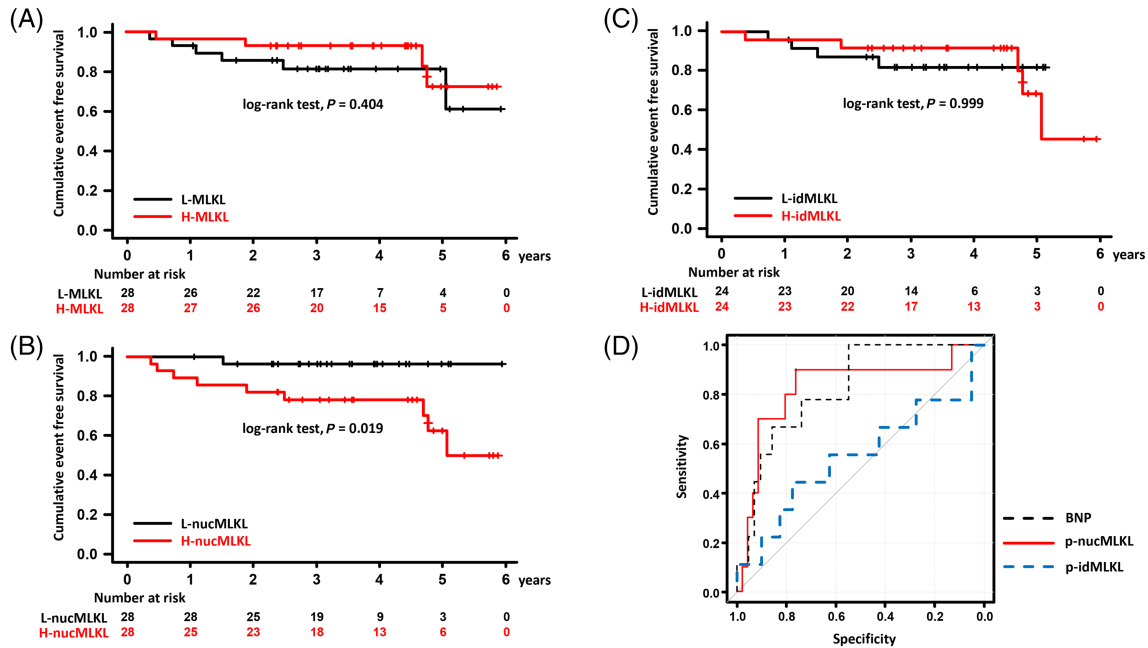
MLKL phosphorylation in an animal model of DCM

Because we could obtain only three cases of normal human myocardial samples for comparison with the DCM samples, we used 36-week-old Sgcd$^{-/-}$ mice and their WT mice to confirm the association of change in p-MLKL expression with DCM. Mice of this age were selected on the basis of their phenotype of ventricular dysfunction similar to DCM[32]; re-

duction in LVEF together with LV enlargement and replacement fibrosis were found in Sgcd$^{-/-}$ mice but not in age-matched WT mice as shown in Supporting Information, *Table S1* and *Figure S5*.

In WT mice, slight p-MLKL signals were detected in the cytosol, but signals were barely observed in the nuclei and intercalated discs of cardiomyocytes (*Figure 5* and Supporting Information, *Figure S6*). In Sgcd$^{-/-}$ mice, an increase in p-MLKL signals was found in the cytosol, intercalated discs, and nuclei of cardiomyocytes (*Figure 5* and Supporting Information, *Figure S6*). p-MLKL signals were increased in cardiomyocytes surrounding replacement fibrosis, a pattern of collagen deposition that occurs following cell necrosis for preservation of structural integrity, in Sgcd$^{-/-}$ mice as in DCM (*Figure 5*). Total p-MLKL and p-nucMLKL levels were significantly higher in Sgcd$^{-/-}$ mice than in WT mice (*Figure 5*). In addition, p-RIP3 levels were also higher in Sgcd$^{-/-}$ mice than in WT mice (Supporting Information, *Table S1* and *Figure S7*). As presented in Supporting Information, *Table S2*, p-nucMLKL level was not correlated with caspase-8 expression level, whereas it was correlated with p-RIP3 level. In addition, p-nucMLKL level was positively correlated with fibrosis area in Sgcd$^{-/-}$ mice (Supporting Information, *Table S2*).

Because slight p-MLKL signals were detected in WT mice in contrast to no signal in normal human samples (*Figure 3F* vs. Supporting Information, *Figure S4A–S4F*), we performed *post hoc* analyses to assess specificities of two antibodies against mouse p-MLKL, MA5-32752 and ab196436, by using C2C12 cells. Immunoblotting with MA5-32752 and that with

Figure 4 Adverse event-free survival curves for different levels of p-MLKL in the myocardium. Kaplan–Meier survival curves for groups divided by the median value of total p-MLKL level, nuclear p-MLKL, or intercalated disc p-MLKL. (A) A high p-MLKL level group (H-MLKL) and a low p-MLKL level group (L-MLKL). (B) A high nuclear p-MLKL (p-nucMLKL) level group (H-nucMLKL) and a low nuclear p-MLKL level group (L-nucMLKL). (C) A high intercalated disc p-MLKL (p-idMLKL) level group (H-idMLKL) and a low intercalated disc p-MLKL level group (L-idMLKL). (D) Receiver operating characteristic curves of brain-type natriuretic peptide (BNP) and p-MLKL levels for predicting adverse events. Area under the curve (AUC) value for each variable is as follows: BNP, 0.823 [95% confidence interval (CI), 0.688–0.958]; p-nucMLKL, 0.826 (95% CI, 0.657–0.995); and p-idMLKL, 0.547 (95% CI, 0.300–0.795).


Discussion

In the present study, noticeable localization of p-MLKL was observed in the nuclei, particularly those that were enlarged and/or had bizarre shapes, and also in the intercalated discs of cardiomyocytes in DCM patients. A high nuclear p-MLKL level in the patients was associated with diastolic dysfunction and was a significant predictor of adverse events during the follow-up period, although the associations may not represent causal relationships. The number of normal human control samples was not large enough to make a statistical comparison with DCM cases. However, an association of increase in nuclear p-MLKL with DCM phenotypes was supported by the results of mice experiments suggesting that nuclear p-MLKL level, which was correlated with fibrosis area, was

ab196436 showed that treatment of C2C12 cells with TNF/zVAD increased a signal that corresponded to p-MLKL, but there were multiple non-specific bands in the blotting in unstimulated cell samples (Supporting Information, *Figure S8*). The results of the *post hoc* experiments suggest that p-MLKL levels were overestimated to some extent by MA5-32752 due to non-specific staining in the mouse immunohistochemistry experiments.

higher in Sgcd$^{-/-}$ mice than in WT mice. To our knowledge, this is the first study showing a significant association of nuclear localization of p-MLKL with clinical outcomes in human diseases.

The mechanism for the association of increased nuclear p-MLKL level with poor clinical outcomes in DCM (*Figure 4*) remains unclear, but several lines of evidence indicate the possibility that nuclear p-MLKL and/or its complex with p-RIP3 contribute to detrimental alterations of chromatin in DCM by modification of the nuclear envelope. Yoon *et al*. found that execution of TNF-α-triggered necroptosis was preceded by the translocation of p-MLKL to the nucleus in fibroblasts.[20] Recently, Weber *et al*. showed that interaction of p-MLKL and p-RIP3 in the nucleus precedes the formation of necrosomes in the cytosol and that inhibition of the nuclear export of MLKL reduced both cytosolic necrosomes and necroptotic cell death.[19] DNA leakage from the disrupted nuclear envelope was reported to be responsible for necroptosis triggered by influenza virus,[37] and dilation of perinuclear spaces in cells undergoing necroptosis was observed by electron microscopy.[38] Contribution of nuclear damage to worsening of clinical outcomes in DCM patients has been suggested by development of DCM by a mutation in a gene encoding lamin A/C, a nuclear envelope protein,[39,40] associations of alterations in nuclear chromatin with ventricular dysfunction and prognosis of DCM,[41,42] and

Figure 5 p-MLKL level in a mouse model of dilated cardiomyopathy. (A, B, D, E) Representative images of the myocardium immunostained with anti-p-MLKL antibodies (MA5-32752) in 36-week-old δ-sarcoglycan-deficient (Sgcd$^{-/-}$) mice and control wild-type (WT) mice. (A, B) WT mice. (D, E) Sgcd$^{-/-}$ mice. Representative images of the myocardium with Masson's trichrome staining in Sgcd$^{-/-}$ mice (F) and WT mice (C). Comparisons of the percentage of p-MLKL-positive areas in the total myocardial area (G) and the percentage of the number of p-MLKL-positive nuclei in the number of total nuclei (H) between WT and Sgcd$^{-/-}$ mice.
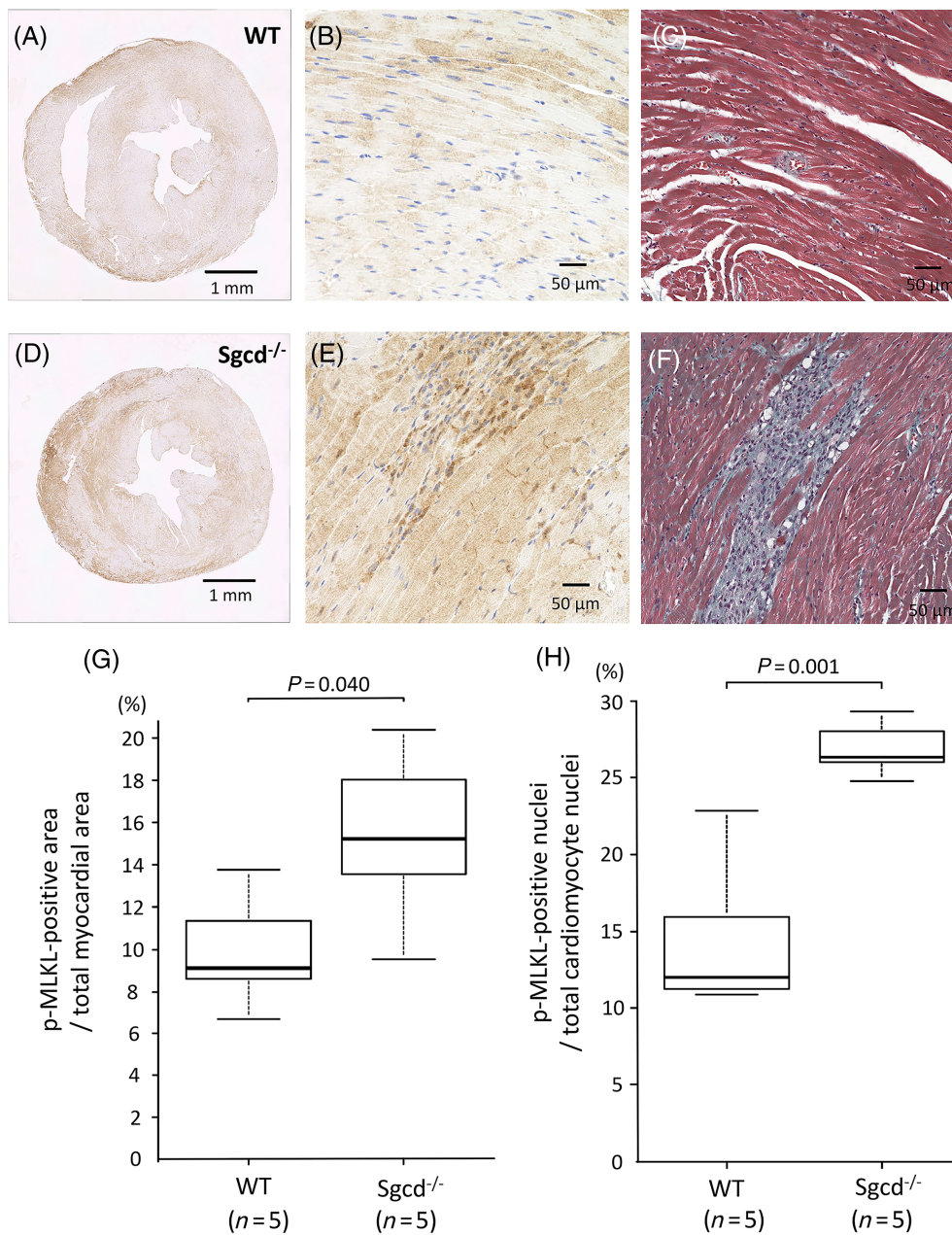
association of DNA damage assessed by using poly(ADP-ribose) and γ-H2A.X as markers with worse clinical outcome after medical therapy in DCM.[43]

The function of activated p-MLKL is not limited to disruption of the plasma membrane and nuclear envelope. Nuclear MLKL contributes to NLRP3 inflammasome formation[44] and also reportedly interacts with RBM6, an RNA-binding protein,

to promote the mRNA stability of adhesion molecules, leading to sustained inflammation.[45] MLKL positively regulates endosomal trafficking and the production of extracellular vesicles independently of the execution of necroptosis.[46] The extracellular vesicles play a role in carrying microRNAs that are possibly involved in the pathogenesis of DCM.[47] In addition, MLKL-dependent activation of the pyruvate dehydrogenase

complex increases production of cytotoxic reactive oxygen species.[48] Some of these actions of activated MLKL might underlie the inverse correlation between nuclear p-MLKL level and e', an index of diastolic function (*Table 3*).

Intracellular behaviour of MLKL throughout the time course of TNF-α-induced necroptosis was extensively analysed by using single-cell imaging approaches in a recent study by Samson *et al*.[49] They showed that p-MLKL was co-trafficked with tight junction proteins to the tight junction during TNF-α-induced canonical necroptosis in HT-29 cells.[49] Similarly to accumulation of p-MLKL at intracellular junctions of HT-29 cells,[49] p-MLKL signals were increased at the intercalated discs rather than the plasma membranes in the DCM myocardium (*Figure 3C–3E*). Taken together, increased localization of p-MLKL in the intercalated discs of the DCM myocardium might reflect activation of necroptotic signalling and modulation of intracellular junctions in the myocardium.

The mechanism of increased p-MLKL level in the myocardium of DCM patients remains unclear. Our attempt by use of four different MLKL antibodies was unsuccessful, and we could not obtain immunohistochemical data for total MLKL in DCM. However, Szobi *et al*.[18] reported that total MLKL levels determined by immunoblotting were comparable between myocardial samples of healthy donors and those of patients with end-stage DCM, while p-MLKL level was significantly higher in myocardial samples of DCM patients than in those of healthy controls. Because total MLKL level was unchanged in DCM patients whose stage of heart failure was more advanced than those in the present study, we speculate that different levels of signal input towards MLKL-Ser358, but not different MLKL protein levels, contribute to the alterations in p-MLKL expression levels in EMB samples.

Consistent with results of an earlier study,[19] p-RIP3 signals were found in the nuclei and were positively correlated with levels of p-MLKL and p-nucMLKL in Sgcd$^{-/-}$ mice (Supporting Information, *Figure S7* and *Table S2*), suggesting that a canonical RIP3-dependent pathway is a possible mechanism of increased nuclear MLKL phosphorylation in DCM. RIP3, the only kinase that has been proved to phosphorylate MLKL, is activated by RIP1-dependent and RIP1-independent pathways,[5] and there is circumstantial evidence indicating that ligands for both RIP1-dependent and RIP1-independent mechanisms of RIP3 activation are increased in patients with heart failure. The most widely investigated trigger event for RIP1-dependent RIP3 activation is stimulation of the TNF-α receptor.[5–7] Levels of plasma TNF-α and other inflammatory cytokines are elevated in patients with heart failure, and the levels correlate with the severity of heart failure. Although clinical trials have failed to show a clinical benefit of TNF-α inhibition for heart failure patients, that does not necessarily exclude a detrimental effect of TNF-α on cardiomyocytes and rather indicates complex functions of TNF-α, including activation of cytoprotective signalling.[50,51]

Reduction of caspase-8 activity is an indispensable event for TNF-α-induced RIP1 phosphorylation, leading to RIP3-dependent MLKL phosphorylation,[5–7,11] but caspase-8 level was not correlated with levels of p-MLKL and nuclear p-MLKL in human DCM (*Table 3*) and Sgcd$^{-/-}$ mice (Supporting Information, *Table S2*). These findings suggest that RIP1-independent RIP3 activation, possibly by damage-associated molecular patterns released from damaged cardiomyocytes or interstitial cells,[5,52,53] contributes to nuclear MLKL phosphorylation in DCM. This possibility is consistent with enhancement of p-MLKL signals in cardiomyocytes surrounding fibrotic foci in EMB samples from DCM patients (*Figure 3*).

There are several limitations in this study. First, the possibility of selection bias in study subjects cannot be excluded because a relatively small number of patients were enrolled in a single centre. Propensity score matching in a *post hoc* analysis of the adverse event rate during the follow-up period was unsuccessful because of the small number of patients in each group. Second, an association between p-MLKL and fibrosis or inflammatory cell infiltration remains unclear. This issue is difficult to analyse by the use of EMB samples because of limited statistical power and sampling bias. Third, we could not quantitate the expression of total MLKL and its localization in the myocardium because a suitable antibody was unavailable. Whether the alterations in p-MLKL expression levels in EMB samples were due to different MLKL protein levels and/or different levels of signal input towards MLKL-Ser358 remains unclear. Fourth, because we could analyse only three cases of normal heart samples, the magnitude of changes in p-MLKL and caspase-8 specifically associated with DCM has not been determined. Fifth, immunohistochemical data for p-MLKL levels in Sgcd$^{-/-}$ mice have not been confirmed by immunoblotting analyses. In addition, antibodies against mouse p-MLKL and p-RIP3 had limited specificities as shown by multiple non-specific bands in immunoblotting in C2C12 cells (Supporting Information, *Figures S8* and *S9*). As recently reported by Samson *et al*.,[54] there are a number of methodological problems regarding frequently used antibodies against MLKL, RIP1, and RIP3 for microscopy studies, and thus, further investigation using a combination of selective antibodies is necessary for full characterization of necroptosis signal pathways in Sgcd$^{-/-}$ mice. Finally, because of a lack of data for time courses of p-MLKL expression and ventricular function, especially diastolic function in DCM patients and Sgcd$^{-/-}$ mice, causal relationships between the two and their relevance to clinical outcomes remain unclear.

In conclusion, immunohistochemical analysis of EMB samples from DCM patients and Sgcd$^{-/-}$ mice indicated that increased MLKL phosphorylation in intracellular compartments of cardiomyocytes is associated with cardiomyopathy. Nuclear p-MLKL level was correlated with diastolic function and predicted future adverse events in DCM patients, while intercalated disc p-MLKL level was correlated with LV wall

thickness. The findings support the notion that activation of necroptotic signalling contributes to progression of DCM via modulation of targets in multiple intracellular compartments.

Supporting information

Additional supporting information may be found online in the Supporting Information section at the end of the article.

Figure S1. Representative images of immunoblotting with ab208909, an anti-p-MLKL-Ser358 antibody, in HT-29 cells. A and B: Representative images of immunoblotting with ab208909 (A), an anti-p-MLKL-Ser358 antibody, and ab184728 (B), an anti-MLKL antibody, in whole cell lysates of HT-29 cells and group mean data for p-MLKL level and MLKL level in cells before and after induction of necroptosis by a combination of 50 ng/ml TNF-α (TNF), 1 μM BV6 and 20 μM Z-Val-Ala-DL-Asp-fluoromethylketone (zVAD). Vehicle (V)-treated cells served as controls. * p<0.05 vs. V. C: Representative immunoblots for p-MLKL-Ser358 in cytosolic and nuclear fractions. Histone-H3 and α-tubulin were used as loading controls of nuclear and cytosolic fractions, respectively.

Figure S2. Representative images of immunohistochemical staining with ab208909, an anti-p-MLKL-Ser358 antibody, in kidney biopsy specimens. (A-D) Representative images of immunoblotting with ab208909, an anti-p-MLKL-Ser358 antibody, in kidney biopsy tissues of lupus nephritis (A, B) and

negative controls (C, D). For the images shown in panels C and D, kidney biopsy tissues of lupus nephritis were incubated with rabbit immunoglobulins as a substitute for ab208909.

Figure S3. Representative images of antibody absorption experiments. Signals of p-MLKL detected by immunostaining with ab208909 in kidney tissues biopsied from a patient with lupus nephritis (A) and in myocardial biopsy tissues of a DCM patient (C) were completely lost by the addition of a blocking peptide prior to the incubation with ab208909 for the purpose of masking the paratope of ab208909: B and D show ab208909-treated kidney and myocardial biopsy tissues, respectively.

Figure S4. Representative images of immunohistochemical staining of human myocardium with ab208909, an anti-p-MLKL-Ser358 antibody, in normal controls and a case of hypertrophic cardiomyopathy. Human tissue samples were obtained from US Biomax (Rockville, MD, # BC30013) and were stained with ab208909. Normal myocardium samples of a 45-year-old man (A, B), a 15-year-old woman (C, D) and a 21-year old woman (E, F) are shown. Panel E is the same photo as panel F in Figure 3. Panels G and H are samples from a 51-year-old woman with hypertrophic cardiomyopathy (HCM). In contrast to cases of DCM shown in Figures 2 and 3, strong signals for p-MLKL in nuclei were not detected in this case of HCM.

Figure S5. Representative images of M-mode echocardiograms of wild-type mice and δ-sarcoglycan-deficient mice. Thirty-six weeks old Wild-type (WT) mice and δ-sarcoglycan-deficient (Sgcd-/-) mice were anesthetized and subjected to transthoracic echocardiography. A, WT mice. B, Sgcd-/- mice. Results of quantitative analyses are presented in Supplementary Table 1.

Figure S6. Representative images of immunohistochemical staining of the myocardium with ab196436, an anti-p-MLKL-Ser345 antibody, in δ-sarcoglycan-deficient mice and wild-type mice. Representative images of the myocardium immunostained with anti-p-MLKL antibodies in 36-week-old control wild-type (WT) mice (A, B) and δ-sarcoglycan-deficient (Sgcd-/-) mice (C, D).

Figure S7. Representative images of immunohistochemical staining of the myocardium with ab222320, anti-p-RIP3-Thr231/Ser232 antibody, in δ-sarcoglycan-deficient mice and wild-type mice. Representative images of the myocardium immunostained with anti-p-RIP3 antibodies in 36-week-old control wildtype mice (A) and δ-sarcoglycan-deficient mice (B).

Figure S8. Representative images of immunoblotting with anti-p-MLKL-Ser345 and anti-MLKL antibodies in C2C12 cells. Representative images of immunoblotting with MA5-32752 (A) and ab196436 (B), anti-p-MLKL-Ser345 antibodies, and ab243142, anti-MLKL antibody, in whole cell lysates of C2C12 cells. C2C12 cells were assigned to 4-hr or 8-hr treatment with a combination of 50 ng/ml TNF-α (TNF) and 20 μM Z-Val-Ala-DL-Asp-fluoromethylketone (zVAD) or a vehicle (V).

Figure S9. Representative images of immunoblotting with anti-p-RIP3-Thr231/Ser232 antibody and anti-RIP3 antibody in C2C12 cells. Representative images of immunoblotting with an anti-p-RIP3-Thr231/Ser232 antibody (ab222320) and anti-RIP3 antibody (#15828) in whole cell lysates of C2C12 cells. C2C12 cells were assigned to 4-hr or 8-hr treatment with the combination of 50 ng/ml TNF-α (TNF) and 20 μM Z-Val-Ala-DL-Asp-fluoromethylketone (zVAD) or a vehicle (V). According to the manufacturer's datasheet, this antibody detects a band of approximately 53 kDa (predicted molecular weight, 57 kDa).

Table S1. Characteristics in a mouse model of dilated cardiomyopathy.

Table S2. Simple regression analyses for MLKL phosphorylation in δ-sarcoglycan-deficient mice.

References

1. McNally EM, Mestroni L. Dilated cardiomyopathy: genetic determinants and mechanisms. *Circ Res*. 2017; **121**: 731–748.

2. Schultheiss HP, Fairweather D, Caforio ALP, Escher F, Hershberger RE, Lipshultz SE, Liu PP, Matsumori A, Mazzanti A, McMurray J, Priori SG. Dilated cardiomyopathy. *Nat Rev Dis Primers*. 2019; **5**: 32.

3. Ushigome R, Sakata Y, Nochioka K, Miyata S, Miura M, Tadaki S, Yamauchi T, Sato K, Onose T, Tsuji K, Abe R, Takahashi J, Shimokawa H, CHART-2 Investigators. Improved long-term prognosis of dilated cardiomyopathy with implementation of evidenced-based medication—report from the CHART studies. *Circ J*. 2015; **79**: 1332–1341.

4. Weintraub RG, Semsarian C, Macdonald P. Dilated cardiomyopathy. *Lancet*. 2017; **390**: 400–414.

5. Grootjans S, Vanden Berghe T, Vandenabeele P. Initiation and execution mechanisms of necroptosis: an overview. *Cell Death Differ*. 2017; **24**: 1184–1195.

6. Linkermann A, Green DR. Necroptosis. *N Engl J Med*. 2014; **370**: 455–465.

7. Lu JV, Chen HC, Walsh CM. Necroptotic signaling in adaptive and innate immunity. *Semin Cell Dev Biol*. 2014; **35**: 33–39.

8. Hein S, Arnon E, Kostin S, Schönburg M, Elsässer A, Polyakova V, Bauer EP, Klövekorn WP, Schaper J. Progression from compensated hypertrophy to failure in the pressure-overloaded human heart: structural deterioration and compensatory mechanisms. *Circulation*. 2003; **107**: 984–991.

9. Kostin S, Pool L, Elsässer A, Hein S, Drexler HC, Arnon E, Hayakawa Y, Zimmermann R, Bauer E, Klövekorn WP, Schaper J. Myocytes die by multiple mechanisms in failing human hearts. *Circ Res*. 2003; **92**: 715–724.

10. Vigliano CA, Cabeza Meckert PM, Diez M, Favaloro LE, Cortés C, Fazzi L, Favaloro RR, Laguens RP. Cardiomyocyte hypertrophy, oncosis, and autophagic vacuolization predict mortality in idiopathic dilated cardiomyopathy with advanced heart failure. *J Am Coll Cardiol*. 2011; **57**: 1523–1531.

11. Abe K, Yano T, Tanno M, Miki T, Kuno A, Sato T, Kouzu H, Nakata K, Ohwada W, Kimura Y, Sugawara H, Shibata S, Igaki Y, Ino S, Miura T. mTORC1 inhibition attenuates necroptosis through RIP1 inhibition-mediated TFEB activation. *Biochim Biophys Acta Mol Basis Dis*. 2019; **1865**: 165552.

12. Ogasawara M, Yano T, Tanno M, Abe K, Ishikawa S, Miki T, Kuno A, Tobisawa T, Muratsubaki S, Ohno K, Tatekoshi Y, Nakata K, Ohwada W, Miura T. Suppression of autophagic flux contributes to cardiomyocyte death by activation of necroptotic pathways. *J Mol Cell Cardiol*. 2017; **108**: 203–213.

13. Luedde M, Lutz M, Carter N, Sosna J, Jacoby C, Vucur M, Gautheron J, Roderburg C, Borg N, Reisinger F, Hippe HJ, Linkermann A, Wolf MJ, Rose-John S, Lüllmann-Rauch R, Adam D, Flögel U, Heikenwalder M, Luedde T, Frey N. RIP3, a kinase promoting necroptotic cell death, mediates adverse remodelling after myocardial infarction. *Cardiovasc Res*. 2014; **103**: 206–216.

14. Guo C, Fu R, Zhou M, Wang S, Huang Y, Hu H, Zhao J, Gaskin F, Yang N, Fu SM. Pathogenesis of lupus nephritis: RIP3 dependent necroptosis and NLRP3 inflammasome activation. *J Autoimmun*. 2019; **103**: 102286.

15. Salem D, Subang R, Pernet E, Divangahi M, Pineau C, Cayrol R, Levine JS, Rauch J. Necroptotic cell binding of β₂-glycoprotein I provides a potential autoantigenic stimulus in systemic lupus erythematosus. *Immunol Cell Biol*. 2019; **97**: 799–814.

16. Nagatomo Y, Tang WH. Autoantibodies and cardiovascular dysfunction: cause or consequence? *Curr Heart Fail Rep*. 2014; **11**: 500–508.

17. Li L, Chen Y, Doan J, Murray J, Molkentin JD, Liu Q. Transforming growth factor β-activated kinase 1 signaling pathway critically regulates myocardial survival and remodeling. *Circulation*. 2014; **130**: 2162–2172.

18. Szobi A, Gonçalvesová E, Varga ZV, Leszek P, Kuśmierczyk M, Hulman M, Kyselovič J, Ferdinandy P, Adameová A. Analysis of necroptotic proteins in failing human hearts. *J Transl Med*. 2017; **15**: 86.

19. Weber K, Roelandt R, Bruggeman I, Estornes Y, Vandenabeele P. Nuclear RIPK3 and MLKL contribute to cytosolic necrosome formation and necroptosis. *Commun Biol*. 2018; **1**: 6.

20. Yoon S, Bogdanov K, Kovalenko A, Wallach D. Necroptosis is preceded by nuclear translocation of the signaling proteins that induce it. *Cell Death Differ*. 2016; **23**: 253–260.

21. Leone O, Veinot JP, Angelini A, Baandrup UT, Basso C, Berry G, Bruneval P, Burke M, Butany J, Calabrese F, d'Amati G, Edwards WD, Fallon JT, Fishbein MC, Gallagher PJ, Halushka MK, McManus B, Pucci A, Rodriguez ER, Saffitz JE, Sheppard MN, Steenbergen C, Stone JR, Tan C, Thiene G, van der Wal AC, Winters GL. 2011 consensus statement on endomyocardial biopsy from the Association for European Cardiovascular Pathology and the Society for Cardiovascular Pathology. *Cardiovasc Pathol*. 2012; **21**: 245–274.

22. Pinto YM, Elliott PM, Arbustini E, Adler Y, Anastasakis A, Böhm M, Duboc D, Gimeno J, de Groote P, Imazio M, Heymans S, Klingel K, Komajda M, Limongelli G, Linhart A, Mogensen J, Moon J, Pieper PG, Seferovic PM, Schueler S, Zamorano JL, Caforio AL, Charron P. Proposal for a revised definition of dilated cardiomyopathy, hypokinetic non-dilated cardiomyopathy, and its implications for clinical practice: a position statement of the ESC Working Group on Myocardial and Pericardial Diseases. *Eur Heart J*. 2016; **37**: 1850–1858.

23. Frustaci A, Russo MA, Chimenti C. Randomized study on the efficacy of immunosuppressive therapy in patients with virus-negative inflammatory cardiomyopathy: the TIMIC study. *Eur Heart J*. 2009; **30**: 1995–2002.

24. Nagano N, Yano T, Fujita Y, Kouzu H, Koyama M, Ikeda H, Yasui K, Muranaka A, Nishikawa R, Takahashi R, Kishiue N, Yuda S, Miura T. Assessment of prognosis in immunoglobulin light chain amyloidosis patients with severe heart

failure: a predictive value of right ventricular function. *Heart Vessels*. 2020; **35**: 521–530.

25. Yano T, Shimoshige S, Miki T, Tanno M, Mochizuki A, Fujito T, Yuda S, Muranaka A, Ogasawara M, Hashimoto A, Tsuchihashi K, Miura T. Clinical impact of myocardial mTORC1 activation in nonischemic dilated cardiomyopathy. *J Mol Cell Cardiol*. 2016; **91**: 6–9.

26. Okada H, Takemura G, Kanamori H, Tsujimoto A, Goto K, Kawamura I, Watanabe T, Morishita K, Miyazaki N, Tanaka T, Ushikoshi H, Kawasaki M, Miyazaki T, Suzui N, Nishigaki K, Mikami A, Ogura S, Minatoguchi S. Phenotype and physiological significance of the endocardial smooth muscle cells in human failing hearts. *Circ Heart Fail*. 2015; **8**: 149–155.

27. Ishikawa K, Kawano Y, Arihara Y, Kubo T, Takada K, Murase K, Miyanishi K, Kobune M, Kato J. BH3 profiling discriminates the anti-apoptotic status of 5-fluorouracil-resistant colon cancer cells. *Oncol Rep*. 2019; **42**: 2416–2425.

28. Peng QL, Zhang YM, Liu YC, Liang L, Li WL, Tian XL, Zhang L, Yang HX, Lu X, Wang GC. Necroptosis contributes to myofiber death in idiopathic inflammatory myopathies. *Arthritis Rheumatol*. 2022 Online ahead of print.

29. Roedig J, Kowald L, Juretschke T, Karlowitz R, Ahangarian Abhari B, Roedig H, Fulda S, Beli P, van Wijk SJ. USP22 controls necroptosis by regulating receptor-interacting protein kinase 3 ubiquitination. *EMBO Rep*. 2021; **22**: e50163.

30. Tsubata S, Bowles KR, Vatta M, Zintz C, Titus J, Muhonen L, Bowles NE, Towbin JA. Mutations in the human *δ-sarcoglycan* gene in familial and sporadic dilated cardiomyopathy. *J Clin Invest*. 2000; **106**: 655–662.

31. Kärkkäinen S, Miettinen R, Tuomainen P, Kärkkäinen P, Heliö T, Reissell E, Kaartinen M, Toivonen L, Nieminen MS, Kuusisto J, Laakso M, Peuhkurinen K. A novel mutation, Arg71Thr, in the δ-sarcoglycan gene is associated with dilated cardiomyopathy. *J Mol Med (Berl)*. 2003; **81**: 795–800.

32. Kanamori H, Naruse G, Yoshida A, Minatoguchi S, Watanabe T, Kawaguchi T, Yamada Y, Mikami A, Kawasaki M, Takemura G, Minatoguchi S. Metformin enhances autophagy and provides cardioprotection in δ-sarcoglycan deficiency-induced dilated cardiomyopathy. *Circ Heart Fail*. 2019; **12**: e005418.

33. Tanno M, Kuno A, Yano T, Miura T, Hisahara S, Ishikawa S, Shimamoto K, Horio Y. Induction of manganese superoxide dismutase by nuclear translocation and activation of SIRT1 promotes cell survival in chronic heart failure. *J Biol Chem*. 2010; **285**: 8375–8382.

34. Heydemann A, Demonbreun A, Hadhazy M, Earley JU, McNally EM. Nuclear sequestration of δ-sarcoglycan disrupts the nuclear localization of lamin A/C and emerin in cardiomyocytes. *Hum Mol Genet*. 2007; **16**: 355–363.

35. Iwata Y, Wakabayashi S, Ito S, Kitakaze M. Production of TRPV2-targeting functional antibody ameliorating dilated cardiomyopathy and muscular dystrophy in animal models. *Lab Invest*. 2020; **100**: 324–337.

36. Hewitt SM, Baskin DG, Frevert CW, Stahl WL, Rosa-Molinar E. Controls for immunohistochemistry: the Histochemical Society's standards of practice for validation of immunohistochemical assays. *J Histochem Cytochem*. 2014; **62**: 693–697.

37. Zhang T, Yin C, Boyd DF, Quarato G, Ingram JP, Shubina M, Ragan KB, Ishizuka T, Crawford JC, Tummers B, Rodriguez DA, Xue J, Peri S, Kaiser WJ, López CB, Xu Y, Upton JW, Thomas PG, Green DR, Balachandran S. Influenza virus Z-RNAs induce ZBP1-mediated necroptosis. *Cell*. 2020; **180**: 1115–1129.e13.

38. Miyake S, Murai S, Kakuta S, Uchiyama Y, Nakano H. Identification of the hallmarks of necroptosis and ferroptosis by transmission electron microscopy. *Biochem Biophys Res Commun*. 2020; **527**: 839–844.

39. Captur G, Arbustini E, Bonne G, Syrris P, Mills K, Wahbi K, Mohiddin SA, McKenna WJ, Pettit S, Ho CY, Muchir A, Gissen P, Elliott PM, Moon JC. Lamin and the heart. *Heart*. 2018; **104**: 468–479.

40. Tobita T, Nomura S, Fujita T, Morita H, Asano Y, Onoue K, Ito M, Imai Y, Suzuki A, Ko T, Satoh M, Fujita K, Naito AT, Furutani Y, Toko H, Harada M, Amiya E, Hatano M, Takimoto E, Shiga T, Nakanishi T, Sakata Y, Ono M, Saito Y, Takashima S, Hagiwara N, Aburatani H, Komuro I. Genetic basis of cardiomyopathy and the genotypes involved in prognosis and left ventricular reverse remodeling. *Sci Rep*. 2018; **8**: 1998.

41. Kanzaki M, Asano Y, Ishibashi-Ueda H, Oiki E, Nishida T, Asanuma H, Kato H, Oka T, Ohtani T, Tsukamoto O, Higo S, Kioka H, Matsuoka K, Sawa Y, Komuro I, Kitakaze M, Takashima S, Sakata Y. A development of nucleic chromatin measurements as a new prognostic marker for severe chronic heart failure. *PLoS One*. 2016; **11**: e0148209.

42. Watanabe T, Okada H, Kanamori H, Miyazaki N, Tsujimoto A, Takada C, Suzuki K, Naruse G, Yoshida A, Nawa T, Tanaka T, Kawasaki M, Ito H, Ogura S, Okura H, Fujiwara T, Fujiwara H, Takemura G. *In situ* nuclear DNA methylation in dilated cardiomyopathy: an endomyocardial biopsy study. *ESC Heart Fail*. 2020; **7**: 493–502.

43. Ko T, Fujita K, Nomura S, Uemura Y, Yamada S, Tobita T, Katoh M, Satoh M, Ito M, Domoto Y, Hosoya Y, Amiya E, Hatano M, Morita H, Fukayama M, Aburatani H, Komuro I. Quantification of DNA damage in heart tissue as a novel prediction tool for therapeutic prognosis of patients with dilated cardiomyopathy. *JACC Basic Transl Sci*. 2019; **4**: 670–680.

44. Conos SA, Chen KW, De Nardo D, Hara H, Whitehead L, Núñez G, Masters SL, Murphy JM, Schroder K, Vaux DL, Lawlor KE, Lindqvist LM, Vince JE. Active MLKL triggers the NLRP3 inflammasome in a cell-intrinsic manner. *Proc Natl Acad Sci U S A*. 2017; **114**: E961–E969.

45. Dai J, Zhang C, Guo L, He H, Jiang K, Huang Y, Zhang X, Zhang H, Wei W, Zhang Y, Lu L, Hu J. A necroptotic-independent function of MLKL in regulating endothelial cell adhesion molecule expression. *Cell Death Dis*. 2020; **11**: 282.

46. Yoon S, Kovalenko A, Bogdanov K, Wallach D. MLKL, the protein that mediates necroptosis, also regulates endosomal trafficking and extracellular vesicle generation. *Immunity*. 2017; **47**: 51–65.e7.

47. Calderon-Dominguez M, Belmonte T, Quezada-Feijoo M, Ramos-Sánchez M, Fernández-Armenta J, Pérez-Navarro A, Cesar S, Peña-Peña L, Vea À, Llorente-Cortés V, Mangas A, de Gonzalo-Calvo D, Toro R. Emerging role of microRNAs in dilated cardiomyopathy: evidence regarding etiology. *Transl Res*. 2020; **215**: 86–101.

48. Yang Z, Wang Y, Zhang Y, He X, Zhong CQ, Ni H, Chen X, Liang Y, Wu J, Zhao S, Zhou D, Han J. RIP3 targets pyruvate dehydrogenase complex to increase aerobic respiration in TNF-induced necroptosis. *Nat Cell Biol*. 2018; **20**: 186–197.

49. Samson AL, Zhang Y, Geoghegan ND, Gavin XJ, Davies KA, Mlodzianoski MJ, Whitehead LW, Frank D, Garnish SE, Fitzgibbon C, Hempel A, Young SN, Jacobsen AV, Cawthorne W, Petrie EJ, Faux MC, Shield-Artin K, Lalaoui N, Hildebrand JM, Silke J, Rogers KL, Lessene G, Hawkins ED, Murphy JM. MLKL trafficking and accumulation at the plasma membrane control the kinetics and threshold for necroptosis. *Nat Commun*. 2020; **11**: 3151.

50. Kleinbongard P, Schulz R, Heusch G. TNFα in myocardial ischemia/reperfusion, remodeling and heart failure. *Heart Fail Rev*. 2011; **16**: 49–69.

51. Mann DL. Innate immunity and the failing heart: the cytokine hypothesis revisited. *Circ Res*. 2015; **116**: 1254–1268.

52. Dhondup Y, Ueland T, Dahl CP, Askevold ET, Sandanger Ø, Fiane A, Ohm IK, Sjaastad I, Finsen AV, Wæhre A, Gullestad L, Aukrust P, Yndestad A, Vinge LE. Nuclear DNA predict mortality in chronic heart failure. *J Card Fail*. 2016; **22**: 823–828.

53. Nakayama H, Otsu K. Mitochondrial DNA as an inflammatory mediator in cardiovascular diseases. *Biochem J*. 2018; **475**: 839–852.

54. Samson AL, Fitzgibbon C, Patel KM, Hildebrand JM, Whitehead LW, Rimes JS, Jacobsen AV, Horne CR, Gavin XJ, Young SN, Rogers KL, Hawkins ED, Murphy JM. A toolbox for imaging RIPK1, RIPK3, and MLKL in mouse and human cells. *Cell Death Differ*. 2021; **28**: 2126–2144.